Spin-wave modes in a cobalt square vortex: Micromagnetic simulations

M. Yan,[1] G. Leaf,[1] H. Kaper,[1] R. Camley,[2] and M. Grimsditch[3]
[1]*Mathematics and Computer Science Division, Argonne National Laboratory, Argonne, Illinois 60439, USA*
[2]*Department of Physics, University of Colorado, Colorado Springs, Colorado 80918, USA*
[3]*Materials Science Division, Argonne National Laboratory, Argonne, Illinois 60439, USA*
(Received 20 September 2005; revised manuscript received 7 December 2005; published 26 January 2006)

Spin-wave modes in a thin submicron cobalt square with a closure domain structure are obtained by using a micromagnetic equation of motion approach. In addition to modes with amplitude over the whole sample, some low-frequency modes, localized at the center, corners, and diagonals of the square, are also found. In analogy with the modes found in a circular vortex, the nonlocalized modes can be broadly classified into radial-like and azimuthal-like modes, and their frequencies can be understood qualitatively in terms of the dispersion relation of spin-wave modes of an unconfined film. Other modes that can be interpreted as the combination of radial and azimuthal modes are also observed.

DOI: 10.1103/PhysRevB.73.014425 PACS number(s): 75.40.Gb

INTRODUCTION

Recent progress in lithographic techniques allows the fabrication of high-quality, well-controlled, laterally defined magnetic structures of micron and submicron sizes. Both the static and dynamic properties of such structures with different geometric shapes are being extensively studied.[1–24] For potential application in high-density storage devices, structures with closure domains have a significant advantage because they have small stray fields and thus reduce the interactions between adjacent elements. The simplest closure domain structure is a circular vortex with perfect cylindrical symmetry. Its excitation spectrum has been studied both theoretically[6,11,19,20] and experimentally.[18,21,23,24] A somewhat more complicated structure is a square particle whose magnetic ground state is a vortex with fourfold symmetry. A few normal modes of square vortex have been revealed experimentally,[15–17,24] but because of the resolution limits of the experiments, the full excitation spectrum is not yet known. To provide a deeper understanding of the properties of a square vortex, we present a theoretical study of its magnetic normal modes.

In submicron-sized magnetic structures, both exchange and dipolar interactions must be taken into account to calculate normal modes. Although the problem is of general interest from a fundamental standpoint, only recently[12,14] have methods for finding the magnetic normal modes in complicated structures (e.g., particles in a vortex ground state) been implemented. To date, no analytical theory has been established to study the full spin-wave spectrum in a square vortex. In this paper, we present a micromagnetic simulation of the spin-wave modes in a cobalt square vortex.

The simulations required solving the Landau-Lifshitz-Gilbert equation numerically as described in Ref. 12. The sample we chose to study is a polycrystalline Co thin film square with a lateral width of 305 nm and a thickness of 20 nm. The magnetic parameters used in the simulation are typical for polycrystalline Co, with the saturation magnetization $\mathrm{Ms}=1400$ emu/cc, exchange stiffness $A=3\times10^{-6}$ ergs/cm, and zero anisotropy. In the simulations, the sample was divided into cubic cells with the cell size equal to 5 nm. At remanence the magnetic ground state of the sample is the closure domain structure shown in Fig. 1.

In order to excite spin-wave modes in the stable ground state, perturbations must be applied to the equilibrium configuration. Using different perturbations in the simulations serves two purposes. First, perturbations with different symmetries excite modes of different symmetries, and thus one can use the form of the perturbation to select a particular class of dynamic modes. Second, exciting only a subset of all normal modes reduces the effects of overlap between modes with similar frequencies. The simplest perturbation is to change the ground-state magnetization profile by uniformly tilting the magnetization in every cell by a small angle. However, to couple to modes with spatially different phases in a particular magnetization component, we divided the square along its diagonals into four triangles, or into four smaller squares along the midpoint of the edges. In each of these subregions the magnetization can be tilted by a different angle. Another type of perturbation is to apply a short magnetic field pulse either in or out of the sample plane. After a perturbation has been applied and the Gilbert damping coefficient has been set to zero, the time evolution of the magnetization of each cell is calculated and stored. A Fourier transform (FT) of the magnetization of each spin then yields its frequency spectrum. The normal mode profile at each frequency can then be reconstructed from the amplitude and phase of the individual FTs. The nature of spin normal modes in square elements has been addressed experimentally in Refs. 15–17 and Ref. 24. Although our aim is to provide a theoretical description of these results, the size of the squares in those investigations ($\approx$1 micron) is larger than we are currently able to simulate. Given our current computing power, we chose to simulate particles 305 nm on a side and 20 nm thick. Hence, although our calculated frequencies are not expected to match those measured in Refs. 15–17 and Ref. 24, the type of modes is expected to be similar, and our results should provide a qualitative guide. We also chose to simulate Co particles because we anticipate that they should provide a stronger coupling in our planned Brillouin scattering measurements. Figure 1(a) shows the results of a simu-

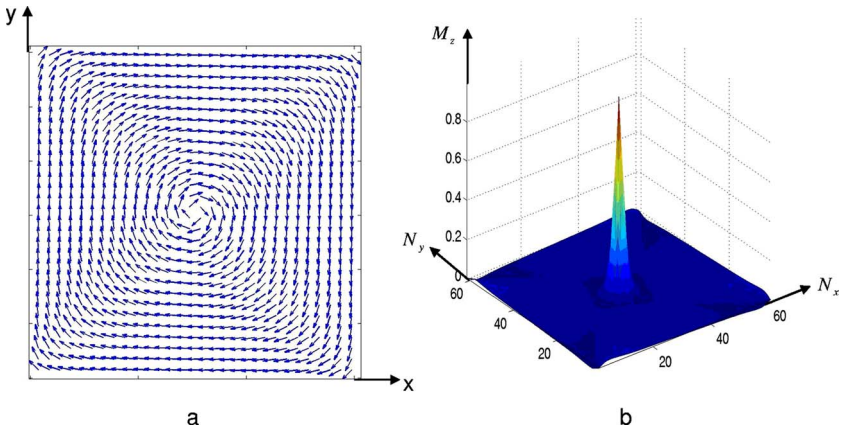

FIG. 1. (Color online) Equilibrium state of the Co square at zero field: (a) in-plane magnetization distribution in the vortex state; (b) out-of-plane component of the magnetization M_z; N_x and N_y are the number of cells in x and y direction, respectively. The magnetization pattern is taken from the second of four layers, but the magnetization variation through the thickness of the film is very small.

lation of the closure domain structure, with a vortex at its center. The magnetization in the ground state is in the film plane everywhere except for the core region, where the magnetization is out of plane, as shown in Fig. 1(b).

The square vortex has some similarity with the vortex found in circular geometries. In the circular vortex the normal modes could be classified into a core mode, radially varying modes, azimuthal varying modes, and combinations of the latter two types.[20,23] The aim of this investigation is to determine how the reduced symmetry of the square affects this classification. The square vortex structure can be viewed as four triangular domains, each of which has a homogeneous magnetization in a different direction [Fig. 1(a)]. However, the magnetization in the vortex core and in the four 90 degree domain walls, which include the four corners, is strongly inhomogeneous and leads to inhomogeneous internal fields in these regions.

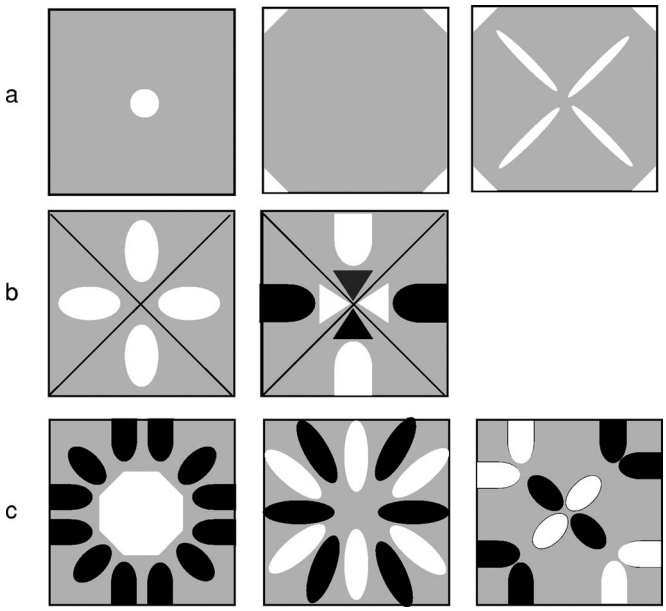

FIG. 2. Sketches of amplitude distribution of different modes observed in a square vortex. Black and white indicate different phases; gray represents negligible amplitude. (a) Mode localized at the core, the corners and diagonals; (b) modes mainly distributed at the four triangular domains; (c) radial-like mode, azimuthal-like mode, and combination of radial-like and azimuthal-like modes.

To discuss the results of this study, we classify the modes into three groups:

(1) low-frequency modes localized in the regions with inhomogeneous fields including the core, domain walls, and corners;

(2) intermediate-frequency modes with amplitudes concentrated in the homogeneous regions of magnetization;

(3) high-frequency modes that resemble more closely the radial and azimuthal character of the modes in a circular disk.

An overview of the amplitude distribution in the three categories is shown schematically in Fig. 2. In the next section, we discuss how we have arrived at this classification scheme.

RESULTS AND DISCUSSION

In this section we give a general overview of the types of modes found in the square vortex and their frequency behavior. A complete characterization of the normal modes of our square vortex would require specifying the frequency and amplitude of all 14 884 modes of our $(61\times61\times4)$ cell particle. Since this would be both impractical and useless, we restrict our presentation to a few selected modes that enable a general classification scheme to be proposed. This scheme provides a guide to the type and frequency of the modes that can be expected in rectangular particles in a closure domain state.

We first briefly review the method of Ref. 12, explaining how we obtain mode profiles and their frequencies and how we present the data. From a perturbed equilibrium ground state we monitor the time evolution of the spin motion in each cell. Since in the equilibrium state the magnetization of most of the cells lies in the plane of the square, a convenient description of a mode is its dynamical, out-of-plane component of the magnetization, in this case, m_z in the coordinate system defined in Fig. 1(a). From the FT of the m_z motion, one finds the amplitude A_i and phase ϕ_i in each cell i as a function of frequency. For a given perturbation, there are typically a number of frequencies where the amplitudes are large; that is, several modes are excited and well resolved. One can find a spatial profile of a mode at a particular frequency ω by plotting $A_i\cos(\phi_i)$ on a square grid representing all the cells. This is equivalent to an instantaneous "snapshot" of the out-of-plane precession for a particular mode at

frequency ω. In the following discussion, we use this snapshot representation to describe the different normal modes produced in our simulations.

Figure 3 shows a snapshot of m_z for the lowest-frequency mode we observed. The color bar on the left applies to all the other snapshot pictures in the sense that redness indicates a positive value and blueness a negative one. As a function of time, the red and blue spots in the image rotate around the center of the square. Clearly, this 0.3 GHz mode is strongly localized at the center of the square and is equivalent to the well-known mode of the precession of the vortex core in circular disks. Since the frequency resolution in our simulation is about 0.3 GHz, the frequency of this mode is accurate only to ±0.15 GHz.

The next-lowest-frequency modes are those with large amplitudes localized at the corners. In a square we may therefore expect four modes of this type—one for each corner. For example, we could have four separate modes with the power localized in a single corner in each mode. In the absence of interactions, these four modes would be degenerate in frequency. However, because of the interactions between the precessing spins in the different corners, in this case resulting primarily from the long-range dipolar interactions, the real solutions will be linear combinations of the single corner states. Figures 4(a)–4(c) show a set of modes localized at the corners of the square. We find the following: a mode with equal amounts of power in all corners and all the corners moving in phase [Fig. 4(a)], a mode with equal amounts of power in all corners, where the corners along one diagonal are in phase with each other but out of phase with the corners along the other diagonal [Fig. 4(b)], and two modes where the power is localized at corners only along one diagonal [Fig. 4(c) shows one of these modes].

The corner mode frequencies are all very close, indicating that the interaction between the corners is small. With our frequency resolution (0.3 GHz), the modes shown in Figs. 4(b) and 4(c) are not resolved. We can explain this behavior with the following argument. For the all-in-phase mode an individual corner sees the dipolar field produced by the three other corners all pointing up at the same time. The sum of these fields produces an additional restoring force that shifts the frequency of this mode slightly upwards. For all the other modes the dipolar fields from the other corners tend to cancel, and an individual corner sees a smaller restoring field. For example, in Fig. 4(b) an individual corner sees two of the remaining corners as up and one as down. Similarly in Fig. 4(c) an individual corner sees the field from the only other active corner.

The mode shown in Fig. 4(c), which is strongly localized at the upper-left and lower-right corners, is degenerate with the mode with amplitude at the two other corners. Because of this degeneracy these modes can be combined with an arbitrary phase. In particular, a right- and left-circularly polarized pair can also be chosen as the basis of these two modes. In a real system it is not clear how imperfections in the sample might select between the two possibilities.

Figures 4(d)–4(f) show the last type of localized mode sketched in Fig. 2(a). Here the mode amplitude is localized primarily along the domain walls that lie along the diagonals. As for the corner modes, the relative phase of the amplitude along each diagonal gives rise to four modes with similar frequencies. In this case the mode in Fig. 4(f) is doubly degenerate. In all three modes shown in Figs. 4(d)–4(f) the amplitude at each corner is out of phase with that on its neighboring diagonal. The 13.2 GHz mode shown in Fig. 4(d) has all four corners in phase with each other but out of phase with the four diagonals. Each corner (or diagonal) of the 11.9 GHz mode shown in Fig. 4(e) is in phase with its opposite one and out of phase with its neighbors. Figure 4(f) shows another mode with different relative phases. This mode can be interpreted as a combination of "circularly polarized" and "single diagonal" modes. All three modes have slightly different frequencies, again primarily the result of dipolar interactions. As we saw in the case of the corner modes, the most in-phase mode, Fig. 4(d), again has the highest frequency.

So far we have discussed the low-frequency modes that are localized in regions with an inhomogeneous equilibrium magnetization including the vortex core, the corners, and the diagonals of the square. We now turn to the type of modes shown in Fig. 2(b) with the amplitude localized in the homogeneous magnetization regions. Figure 5(a) shows a mode with its amplitude concentrated within the four domains. There is no node in any direction in this mode because all regions with nonzero amplitude are in phase. This mode can therefore be viewed as the "uniform resonance" mode and is expected to be the strongest mode in ferromagnetic resonance experiments. From the earlier discussion on the corner modes, one should also expect to find modes where the power distribution is similar to that seen in Fig. 5(a), but the phase relationships between the excitations in each of the four domains is not that of the uniform mode. We do, in fact, find modes at slightly lower frequencies as expected, but they appear to be hybrids, with modes of the type shown in Fig. 2(a) with multiple nodes along each diagonal. Figure 5(b) shows another mode localized in the homogeneous regions, but this mode has one node between the center and the edge.

To understand the modes in our third category, we first recall that the normal modes in a circular vortex with perfect symmetry[20,23] can be characterized as radial modes, azimuthal modes, and combinations of these two types. These modes have been calculated theoretically[20,23] and observed in experiments.[18] A square vortex loses the perfect symmetry of a circular vortex but maintains a fourfold symmetry. In our simulation of a square vortex, we again find some modes that can be classified into radial [Figs. 6(a)–6(d)] and azimuthal [Figs. 6(e)–6(g)]. We discuss the behavior of these modes below.

Figures 6(a)–6(d) show the radial-like modes observed in our simulations. As shown in Fig. 6(a), the amplitude of the 24.5 GHz mode is distributed at the center and around an outer circle. Instead of being continuous along the azimuthal direction as in a circular vortex, the mode is discretized in a pattern consistent with the symmetry of the square vortex. Since there is a phase difference of π between the central and outer part, we can define a radial nodal line in this mode. Figures 6(b) and 6(c) show the modes with two and three nodal lines. Even the mode with four nodal lines is well resolved in our simulation, as shown in Fig. 6(d). The fre-

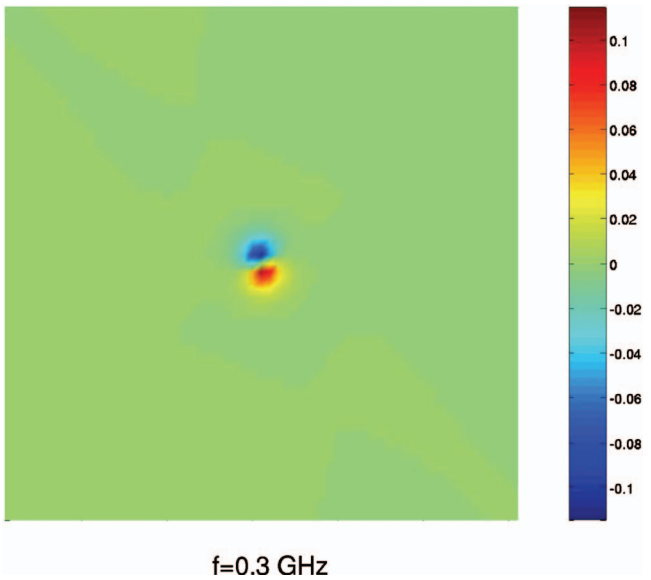

FIG. 3. (Color) Snapshot of the dynamical out-of-plane component of the magnetization m_z for the lowest-frequency mode localized at the vortex core. Note that the red and blue spots in the image rotate around the center of the square with time, which is not demonstrated by the snapshot at a particular instant. The color bar on the right also applies to the following snapshot pictures in the sense that redness means positive values and blueness negative values.

quency of the radial-like mode increases as the number of nodes is increased, as is seen in Fig. 7(a). This result is consistent with the behavior of spin-wave frequencies in an extended magnetic film, as we shall see below.

Figures 6(e)–6(g) show several of the azimuthal-like modes observed in our simulations. The key characteristic of this class of modes is that the phase changes as one circles around the center of the square. We characterize a mode by counting the number of nodes around the circumference of the square. Figures 6(e)–6(g) show the modes with 12, 20, and 32 nodes, respectively. We have probably missed a lot of azimuthal-like modes in our simulations. Nonetheless, a pattern for frequency as a function of number of nodes emerges

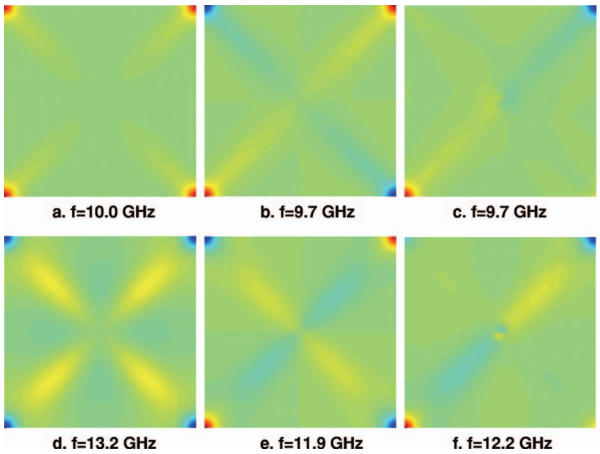

FIG. 4. (Color) Snapshots of the dynamical out-of-plane component of the magnetization m_z for modes localized at corners (a)–(c) and along diagonals (d)–(f).

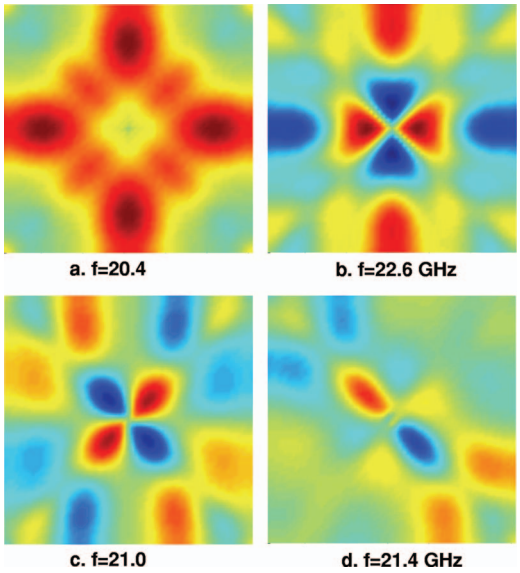

FIG. 5. (Color) Snapshots of the dynamical out-of-plane component of the magnetization m_z for modes mainly distributed at the four triangular domains (a), (b) and for combination of radial-like and azimuthal-like modes (c), (d).

clearly, as can be seen in Fig. 7(b). The frequency of the azimuthal-like modes initially decreases and then increases as the number of nodes increases. Both dipolar and exchange interactions play roles in this situation, as will be discussed below.

To understand the frequency behavior of the radial-like and azimuthal-like modes, we compare the results of Fig. 7 to the dispersion relation in ferromagnetic thin films. In each plot, the first data point corresponds to the uniform mode with no nodes. For the radial-like modes the frequency increases monotonically as the number of the nodes increases. This behavior is similar to the behavior of the Damon-Eshbach mode[25] with wave vectors perpendicular to the static magnetization. With regard to the magnetization distribution of the square vortex, the radial-like modes also change phase in a direction perpendicular to the magnetization. In the case of the Damon-Eshbach mode in an extended ferromagnetic film, the dipolar fields cause the initial in-

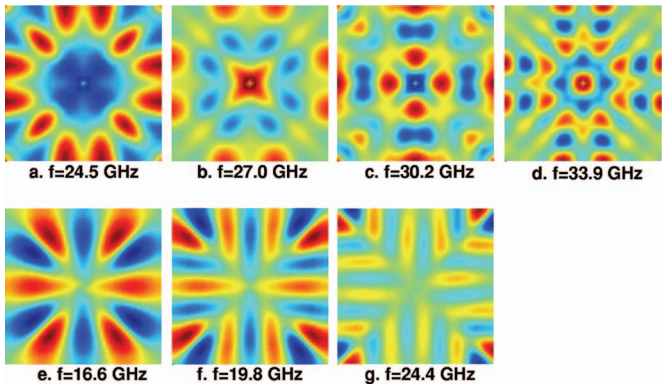

FIG. 6. (Color) Snapshots of the dynamical out-of-plane component of the magnetization m_z for radial-like modes (a)–(d) and for azimuthal-like modes (e)–(g).

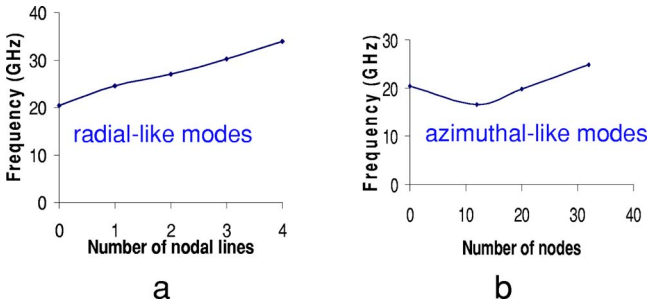

FIG. 7. (Color online) (a) Frequency of the radial-like modes as a function of the number of radial lines; (b) frequency of the azimuthal-like modes as a function of number of nodes.

crease in frequency as the number of nodes (or equivalently propagation wave vector) increases. In the present case the exchange interaction also contributes to the overall frequency increase. For the azimuthal-like modes, the frequency decreases at first and then increases as the number of nodes increases. This behavior is similar to the behavior of the backward volume modes, in which case the wave vector is parallel to the static magnetization. The azimuthal-like modes change phase around the center of the square, which is parallel to the static magnetization of a square vortex. With a small number of nodes, the dipolar interactions are important, and the frequency decreases at first. This behavior is similar to the negative dispersion observed experimentally and calculated analytically with only the dipolar interaction taken into account in larger circular vortices.[20] With a larger number of nodes, the exchange interaction becomes more important, and the frequency increases. Although only a small number of data points are shown in Fig. 7, the frequency behavior of the radial-like and azimuthal-like modes qualitatively mirror the features of equivalent modes in unconfined ferromagnetic thin films.

In our simulations, we also observed modes that can be interpreted as a combination of radial-like and azimuthal-like modes, as shown in Figs. 5(c) and 5(d). Both of those modes change phase, not only radially, but also around the center. Compared to the radial-like mode with just one nodal line as shown in Fig. 6(a), both of these modes have lower frequencies as a result of the dipolar interaction.

MODE SYMMETRIES

The modes presented in the preceding section can also be classified according to their symmetry determined by group theory. The symmetry of the vortex ground state in a square particle is C_4. In assigning this symmetry it must be remembered that the magnetization, being an axial vector, reverses sign under improper symmetry operations such as reflections. Due to this it can be seen that mirror planes that appear to be symmetry operations at first glance actually produce either a change in chirality or of polarity and hence are not symmetry operations of the magnetic ground state. The character table for the C_4 group is shown in Table I and is particularly interesting since the two components of the E mode are only degenerate if time reversal is a symmetry operation. In the case of our magnetic sample this is not the case and hence special care must be taken in assigning the modes.

TABLE I. Character tables for C_4 and C_{4v} groups.

C_4	E	C_2	C_4	C_4^3	
A	1	1	1	1	
B	1	1	−1	−1	
E	1	−1	i	$-i$	
E	1	−1	$-i$	i	
C_{4v}	E	C_2	C_{4+-}	σ_x,σ_y	σ_1,σ_2
A_1	1	1	1	1	1
A_2	1	1	1	−1	−1
B_1	1	1	−1	1	−1
B_2	1	1	−1	−1	1
E	2	−2	0	0	0

We begin with the modes in Figs. 4(a)–4(c). The mode shown in (a) clearly has the full symmetry of the system and hence is an A mode. The mode in (b) changes sign under C_4 operations and is hence a B mode. The mode in (c) is, experimentally, one of a degenerate pair and hence is an E mode. Strictly speaking Table I predicts that the two E modes should be nondegenerate and chiral, differing only in their $\pm\pi/2$ phase difference along the two diagonals.

The modes in Figs. 4(d)–4(f) follow the same classification as those in Figs. 4(a)–4(c). Similarly the modes in Figs. 5(a) and 5(b) are of A and B symmetry, respectively, while all those in Figs. 6(a)–6(d) belong to the A representation. The modes in Figs. 6(e)–6(g) have B, B, and A symmetry and those in Figs. 5(c) and 5(d) belong to the B and E classification. We note that within the accuracy of the simulations all the E modes discussed above appear as pairs whose frequencies are not resolved.

The most interesting mode is, however, the one in Fig. 3 that can be identified as one component of the E doublet. In this case the pattern rotates clockwise as a function of time. The other component of the E doublet in this case does not exist: there is no equivalent mode that rotates counterclockwise. We stress that there is no reason why such a mode must exist.

In this context of mode classification it is instructive to consider the case of a square particle with a round or square hole in the center. If the vortex core is eliminated with such a scheme, the particle acquires C_{4v} symmetry with its resulting character table also shown in Table I. In this case the E modes are strictly degenerate and no intrinsically chiral modes are expected to be present in the system. In this particular case there can be no mode similar in character to that found in cylindrical dots and shown here in Fig. 3 for a square particle.

COMPARISON WITH PREVIOUS EXPERIMENTS AND SIMULATIONS

Excitations in a square vortex have been observed in several experiments.[15–17,24] Our simulation results confirm most of the experimental observations. The vortex core precession

mode (Fig. 3) and modes localized at the corners of the square (Fig. 4) obtained in our simulations were not observed in any of the experiments.[15–17,24] Motion of the vortex core was observed in Raabe's experiment (Fig. 2 of Ref. 17), but its resonance frequency was not determined. The fact that the corner and core modes were missing in these experiments on square vortices[15–17,24] may be due to several reasons. First, since the samples studied in those experiments were larger than those simulated here, the frequencies may have been too low to be resolved. The data in Raabe's experiment shows that the motion of the vortex core is indeed much slower than that of the domain walls.[17] Both the size and the material of the samples studied in experiments imply even lower frequencies than those in our simulations. Second, the spatial resolution in the experiments was not fine enough to resolve these highly localized modes. The third reason that the corner modes are missing in experiments may be due to the effect of edge roundness of the experimentally investigated square samples. The corner modes observed in simulations are localized in small regions of a few tens of nm, which is comparable to the resolution of the lithographic processing.

The domain wall modes, however, were observed in all the experiments,[15–17,24] and they have lower frequencies than do the modes with amplitude over the whole square. This fact is consistent with our results. As illustrated in our simulations, the domain wall modes can have different phases along the four diagonals. It is not clear which of these have been observed in the experiments.

Different numbers of the nonlocalized modes were observed in the experiments.[15–17,24] In Park's experiment,[16] only one was resolved, and it corresponds to the uniform mode with the out-of-plane component at the upper and lower triangular domains out of phase. Up to five such modes were observed in Perzlmaier's experiment.[15] Besides the uniform mode, three "transversal quantized" modes are equivalent to our "radial-like" modes and one "longitudinal quantized" mode is equivalent to our "azimuthal-like" mode. The relative frequencies of these modes are also consistent between the experiment and our simulation. In Raabe's experiment,[17] two modes with the same spatial distribution but different frequencies and initial phases were observed. This phenomenon cannot be explained on the basis of our simulations. The experimental data shows that the in-plane component at the upper and lower triangular domains is in phase in these two modes.[17] Thus, the out-of-plane component at the upper and lower triangular domains should be out of phase. Indeed, two possible modes satisfy this condition with different phase patterns at the left and right triangular domains. But the frequency of these two modes should be degenerate, which is not consistent with the experiment. This could be due to nonlinear effects, as suggested in Ref. 17. In our simulations, the uniform mode with the out-of-plane component of all four triangular domains in phase is well resolved as shown in Fig. 5(a). However, the modes concentrated in triangular domains but out of phase are not resolved. Considering the dipolar interaction among each domain, those modes are expected to have lower frequencies than that of the in-phase mode. In this frequency range, there exist many modes with the amplitude localized along the diagonals. It is likely that the out-of-phase modes in the triangular domains are hybridized with the diagonal modes, so that the profiles of the out-of-phase modes are distorted and cannot be resolved in the simulations. The hybridization effect should be more important in our relatively small sample than the large samples in experiments,[16,17] where out-of-phase modes are indeed observed.

In Ref. 16 and Ref. 24, the magnetic normal modes of square vortices were also studied theoretically using micromagnetic simulations with larger sample sizes (2 μm to 10 μm in Ref. 16 and 4 μm in Ref. 24) and different material parameters (permalloy in both Ref. 16 and Ref. 24). The cell size used in Ref. 16 (12.5 nm) and Ref. 24 (10 nm) are larger than that in our simulations (5 nm). In those simulations, two modes are reported, a lower frequency mode concentrated in the domain walls, which is similar to those reported by us in Figs. 4(d)–4(f), and a higher frequency mode concentrated in the domains.

SUMMARY AND CONCLUSIONS

Using a micromagnetic simulation approach, we have studied the spin-wave modes in a submicron cobalt square sample with a closure domain structure. Several different modes were observed. Low-frequency modes are localized in the inhomogeneous regions, namely, the core, the corners, and the diagonals. The core mode is equivalent to the well-known core precession mode in cylindrical dots. Both the corner and diagonal modes form a closely spaced set of modes with different phase patterns. These modes are not present in cylindrical particles. The uniform mode is equally distributed over the four closure domains. More complicated modes can be classified into radial-like modes and azimuthal-like modes in analogy to the modes in a circular vortex. Because of the reduced symmetry, those modes have more internal structure than in a circular dot. The frequency behavior of the radial-like modes and azimuthal-like modes can be understood qualitatively in terms of the dispersion relation of spin-wave modes of an unconfined film. We also observed some other modes that can be interpreted as the combination of a radial-like mode and an azimuthal-like mode.

We have also reproduced the calculations of magnetic normal modes in a square vortex using a dynamical matrix approach as described in Ref. 14. The results of the two approaches agree well with each other and the field dependence of mode frequencies obtained by the dynamical matrix approach will be discussed in a later paper.

ACKNOWLEDGMENTS

The work of three of the authors (M.Y., G.L., and H.K.) was supported by the Mathematical, Information, and Computational Sciences Division subprogram of the Office of Advanced Scientific Computing Research, Office of Science, U.S. Department of Energy, under Contract No. W-31-109-Eng-38. One of the authors (M.G.) was supported by the Basic Energy Sciences/Materials Sciences program of the U.S. Department of Energy, under Contract No. W-31-109-Eng-38. The work of one of the authors (R.C.) was supported by the Argonne Theory Institute.

[1] W. K. Hiebert, A. Stankiewicz, and M. R. Freeman, Phys. Rev. Lett. **79**, 1134 (1997).
[2] C. Mathieu, J. Jorzick, A. Frank, S. O. Demokritov, A. N. Slavin, B. Hillebrands, B. Bartenlian, C. Chappert, D. Decanini, F. Rousseaux, and E. Cambril, Phys. Rev. Lett. **81**, 3968 (1998).
[3] Y. Acremann, C. H. Back, M. Buess, O. Portmann, A. Vaterlaus, D. Pescia, and H. Melchior, Science **290**, 492 (2002).
[4] S. O. Demokritov, B. Hillebrands, and A. N. Slavin, Phys. Rep. **348**, 441 (2001).
[5] V. Novosad, M. Grimsditch, K. Y. Guslienko, P. Vavassori, Y. Otani, and S. D. Bader, Phys. Rev. B **66**, 052407 (2002).
[6] B. A. Ivanov and C. E. Zaspel, Appl. Phys. Lett. **81**, 1261 (2002).
[7] J. Jorzick, S. O. Demokritov, B. Hillebrands, M. Bailleul, C. Fermon, K. Y. Guslienko, A. N. Slavin, D. V. Berkov, and N. L. Gorn, Phys. Rev. Lett. **88**, 047204 (2002).
[8] J. P. Park, P. Eames, D. M. Engebretson, J. Berezovsky, and P. A. Crowell, Phys. Rev. Lett. **89**, 277201 (2002).
[9] M. Yan, J. Berezovsky, P. A. Crowell, and C. E. Campbell, *Condensed Matter Theories*, edited by M. D. Das and F. Green (Nova Scientific, New York, 2002), Vol. 17.
[10] M. Bailleul, D. Olligs, and C. Fermon, Phys. Rev. Lett. **91**, 137204 (2003).
[11] M. Buess, Y. Acremann, A. Kashuba, C. H. Back, and D. Pescia, J. Phys.: Condens. Matter **15**, 1093 (2003).
[12] M. Grimsditch, G. K. Leaf, H. G. Kaper, D. A. Karpeev, and R. E. Camley, Phys. Rev. B **69**, 174428 (2004).
[13] C. Bayer, J. P. Park, H. Wang, M. Yan, C. E. Campbell, and P. A. Crowell, Phys. Rev. B **69**, 134401 (2004).
[14] M. Grimsditch, L. Giovannini, F. Montoncello, F. Nizzoli, G. K. Leaf, and H. G. Kaper, Phys. Rev. B **70**, 054409 (2004).
[15] K. Perzlmaier, M. Buess, C. H. Back, V. E. Demidov, B. Hillebrands, and S. O. Demokritov, Phys. Rev. Lett. **94**, 057202 (2005).
[16] J. P. Park, P. Eames, D. M. Engebretson, J. Berezovsky, and P. A. Crowell, Phys. Rev. B **67**, 020403(R) (2003).
[17] J. Raabe, C. Quitmann, C. H. Back, F. Nolting, S. Johnson, and C. Buehler, Phys. Rev. Lett. **94**, 217204 (2005).
[18] M. Buess, R. Hollinger, T. Haug, K. Perzlmaier, U. Krey, D. Pescia, M. R. Scheinfein, D. Weiss, and C. H. Back, Phys. Rev. Lett. **93**, 077207 (2004).
[19] B. A. Ivanov and C. E. Zaspel, Phys. Rev. Lett. **94**, 027205 (2005).
[20] M. Buess, T. P. J. Knowles, R. Höllinger, T. Haug, U. Krey, D. Weiss, D. Pescia, M. R. Scheinfein, and C. H. Back, Phys. Rev. B **71**, 104415 (2005).
[21] M. Buess, T. Haug, M. R. Scheinfein, and C. H. Back, Phys. Rev. Lett. **94**, 127205 (2005).
[22] R. D. McMichael and M. D. Stiles, J. Appl. Phys. **97**, 10J901 (2005).
[23] L. Giovannini, F. Montoncello, F. Nizzoli, G. Gubbiotti, G. Carlotti, T. Okuno, T. Shinjo, and M. Grimsditch, Phys. Rev. B **70**, 172404 (2004).
[24] H. Stoll, A. Puzic, B. van Waeyenberge, P. Fischer, J. Raabe, M. Buess, T. Haug, R. Höllinger, C. Back, D. Weiss, and G. Denbeaux, Appl. Phys. Lett. **84**, 3328 (2004).
[25] R. W. Damon and J. R. Eshbach, J. Phys. Chem. Solids **19**, 308 (1961).